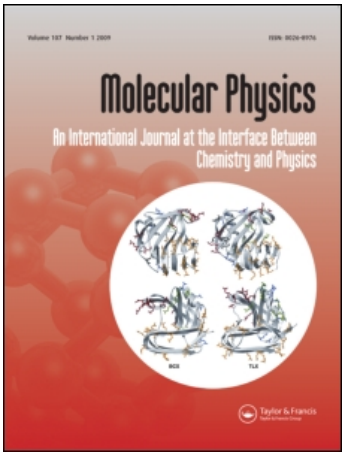

Molecular Physics
Publication details, including instructions for authors and subscription information:
http://www.informaworld.com/smpp/title~content=t713395160

Binary hard-sphere mixtures: a comparison between computer simulation and experiment

M. D. Eldridge[a]; P. A. Madden[a]; P. N. Pusey[b]; P. Bartlett[c]
[a] Physical Chemistry Laboratory, University of Oxford, Oxford, UK [b] Department of Physics and Astronomy, University of Edinburgh, Edinburgh, UK [c] School of Chemistry, University of Bath, Bath, UK

To cite this Article Eldridge, M. D. , Madden, P. A. , Pusey, P. N. and Bartlett, P.(1995) 'Binary hard-sphere mixtures: a comparison between computer simulation and experiment', Molecular Physics, 84: 2, 395 — 420
To link to this Article: DOI: 10.1080/00268979500100271
URL: http://dx.doi.org/10.1080/00268979500100271

MOLECULAR PHYSICS, 1995, VOL. 84, NO. 2, 395–420

Binary hard-sphere mixtures: a comparison between computer simulation and experiment

By M. D. ELDRIDGE, P. A. MADDEN
Physical Chemistry Laboratory, University of Oxford, South Parks Road, Oxford OX1 3QZ, UK

P. N. PUSEY
Department of Physics and Astronomy, University of Edinburgh, Mayfield Road, Edinburgh EH9 3JZ, UK

and P. BARTLETT
School of Chemistry, University of Bath, Claverton Down, Bath BA2 7AY, UK

(*Received 31 August 1994; revised version accepted 11 October 1994*)

The complex crystalline order, recently observed by Bartlett, P., Ottewill, R. H., and Pusey, P. N., 1992, *Phys. Rev. Lett.*, **68**, 3801, in asymmetric binary hard-sphere mixtures is discussed in detail. Experimental observations on phase separation in a complex fluid, a binary suspension of near hard-sphere colloids, are compared with phase diagrams obtained from computer simulations of an atomic hard-sphere liquid. Although there is in general a close degree of agreement between experiment and theory, a detailed comparison shows several unexpected differences. These differences are shown to reflect non-equilibrium effects, and possible reasons for their origin are evaluated.

1. Introduction

This paper concerns the phase behaviour and structure of binary mixtures of hard spheres of different sizes, i.e. large 'A' spheres and small 'B' spheres. We compare the findings of recent experiments on mixtures of 'hard-sphere' colloids, in which binary 'superlattice' crystals AB_2 and AB_{13} were found, with the predictions of recent computer simulations.

Ever since the pioneering work of Bernal [1] and Scott [2], assemblies of hard spheres have been studied quantitatively as models of fluids [3], crystals [4–6] and glasses [7]. Despite the simplicity of the hard-sphere interaction, which lacks both attraction and directionality, hard-sphere systems show many of the properties of real matter. A surprising finding of early computer simulations [3, 4] was that, as their concentration is increased, equal-sized hard spheres undergo a first-order freezing transition to form a crystal with a close-packed structure. Since the internal energy of an assembly of hard spheres is entirely kinetic, this transition must be driven entropically [8–10]. More recent work has established that the hard-sphere freezing transition results from competition between two contributions to the system's entropy, the configurational entropy and the entropy associated with the amount of local free volume available to the spheres. At high concentrations, efficient ordered packings, which provide greater free volume than amorphous packings, are preferred thermodynamically.

0026-8976/95 $10.00

As shown by Bernal [1], the maximum packing or volume fraction of an amorphous assembly of hard spheres is $\phi \simeq 0{\cdot}64$ ('random close packing'). At this concentration the particles are completely constrained by their neighbours and have no free volume for local motions. By contrast, in a crystal at $\phi \simeq 0{\cdot}64$ the particles have considerable free volume, since the concentration of a fully compressed close-packed crystal of hard spheres is $\phi = 0{\cdot}74$. Thus, from the discussion above, one might expect hard spheres to freeze at a concentration $\phi \leqslant 0{\cdot}64$. The computer simulations of Hoover and Ree [4] indeed revealed a first-order freezing transition: the maximum (freezing) volume fraction of an equilibrium hard-sphere fluid is $\phi_F = 0{\cdot}494$ and the minimum (melting) concentration of the hard-sphere crystal is $\phi_M = 0{\cdot}545$.

Implicitly adopting the idea that the freezing of hard-sphere systems is driven by maximizing free-volume entropy, Murray and Sanders [11, 12] considered possible superlattice structures for binary mixtures. They argued that such structures would be stable if their maximum volume fractions (i.e. their free volumes when fully compressed) exceeded 0·74, thus ensuring large free volumes at the lower freezing concentrations; otherwise phase separated crystals of pure A and pure B would be favoured. For radius ratios $\alpha = R_B/R_A$ between 0·3 and 1, Murray and Sanders identified two superlattices AB_2 and AB, which fulfilled this criterion, and one AB_{13}, which marginally failed it. A convenient comparison of close packed densities for binary solids is given in [13]. AB_2 (atomic analogue aluminium and other borides) consists of a hexagonal close packed structure of large A particles with B particles filling the holes between the planes; it has a fully compressed packing fraction greater than 0·74 for $0{\cdot}482 \leqslant \alpha \leqslant 0{\cdot}624$ with a maximum of 0·779 at $\alpha = 0{\cdot}577$. In AB_{13} (atomic analogues $NaZn_{13}$, UBe_{13}) the large spheres are located on a simple cubic lattice and 13 small spheres lie inside the cubic subcells arranged on the vertices of a regular icosahedron; these isocahedra are rotated by 90° between adjacent cubic subcells so that the unit cell of this complex structure comprises 8 subcells containing 112 particles. The maximum packing fraction of AB_{13} is found to be 0·738 at $\alpha = 0{\cdot}558$. For the size ratios of interest in the present work, $0{\cdot}5 \leqslant \alpha \leqslant 0{\cdot}65$, AB_2 and AB_{13} are the phases which might possibly be stable with respect to the pure solids. Outside this range other structures are possible. The sodium chloride structure AB has a maximum packing fraction of 0·793 at $\alpha = 0{\cdot}414$; its stability for small size ratios, $\alpha \leqslant 0{\cdot}45$, has been established elsewhere [14]. At very high size ratios, $\alpha \geqslant 0{\cdot}85$, a random alloy with a close-packed structure is the preferred structure [15, 16]. In the range $0{\cdot}65 \leqslant \alpha \leqslant 0{\cdot}85$ it seems likely that phase separation of the pure solids will occur at high concentrations; formation of an AB solid with the CsCl structure has been discounted after thermodynamic considerations similar to those described later [17].

Most studies of the thermodynamic and structural properties of hard-sphere assemblies have been theoretical or by computer simulation rather than experimental. In the ball bearing experiments gravitational forces completely dominate thermal excitations; on the other hand, hard-sphere atoms, which would show thermal motion, do not exist. Over the last few years, however, a number of experiments have been performed on suspensions of sub-micron-sized colloidal spheres, whose interaction is steep and repulsive and is well approximated by that of hard spheres, which show significant Brownian motion [18, 19]. These suspensions can thus reach thermodynamic equilibrium (although in some cases special measures must be taken to reduce residual gravitational effects). The initial experiments established the phase

behaviour [20] and the structure and dynamics of the fluid, crystalline and glassy states of suspensions of (nearly) equal sized particles [18]. Later Bartlett, Ottewill and Pusey [21, 22] investigated binary mixtures identifying both the AB_2 and AB_{13} structures. Two mixtures were studied at size ratios $\alpha = 0{\cdot}62 \pm 0{\cdot}01$ and $\alpha = 0{\cdot}58 \pm 0{\cdot}01$. Motivated in part by these experiments, Eldridge, Madden and Frenkel calculated the free energies of the AB_2 [23] and AB_{13} [24] structures and constructed a theoretical phase diagram for the binary mixtures at $\alpha = 0{\cdot}58$ [25].

We draw attention to some special properties of colloidal suspensions. The liquid in which the particles are suspended can, to a good approximation, be regarded as an incompressible thermal reservoir. Thus, so far as its thermodynamic properties are concerned, a binary suspension can be treated as a two-component, A and B, system. If it is further assumed that the particles are also incompressible, a colloidal suspension is studied under conditions of constant volume. This contrasts with the more common experimental situation where the external constraint is one of constant pressure. Bartlett [26] has suggested that the phase diagram of a binary mixture at constant volume is most naturally represented in a 'density–density' form in which the axes are ϕ_A and ϕ_B, the partial volume fractions of the components. In this representation, three-phase eutectic triangles replace the eutectic points of the usual pressure–composition or temperature–composition representations (see figure 1(*a*) and the discussion in section 3).

The main purpose of this paper is to compare the experimental findings with the predictions of computer simulation, presenting in the process more complete experimental and theoretical phase diagrams than in previous publications. While there is a broad level of agreement between experiment and simulation (and, furthermore, with the arguments of Murray and Sanders), there are several differences of detail. In particular, we note that the icosahedral-containing superlattice phase AB_{13} is formed more readily from a fluid than equilibrium simulations predict and, second, that mixtures in which there is a marked difference in composition between the predicted equilibrium crystal and the fluid phase are often observed experimentally to form amorphous solids. We believe that these relatively minor disagreements are *not* caused by the failure of the hard-sphere model to represent the potential between the polymethylmethacrylate (PMMA) colloidal particles used in these experiments (see section 2.1). Indeed, our philosophy in writing this paper is to assume that these discrepancies reflect the importance of non-equilibrium factors which, although undoubtedly present in our experiments, are absent from the equilibrium computer simulations. The importance of such kinetic factors in the crystallization of one-component hard sphere is well documented. For example, at $\phi \sim 0{\cdot}58$, a glass transition suppresses long distance diffusion in a one-component assembly of hard spheres and prevents homogeneous nucleation [7]. In experiments, colloidal samples with $\phi > 0{\cdot}58$ do eventually crystallize but only by a process of heterogeneous nucleation at a rate which is much smaller than the homogeneously nucleated crystallization observed at lower concentrations. Obviously these non-equilibrium effects will also operate in mixtures. Indeed one could envisage that the consequences of such non-equilibrium transitions would be more complex than the simple suppression of crystallization observed in a one-component system. In an asymmetric binary mixture there is the additional possibility of a 'selective' arrest of just one of the two component species (i.e. a 'partial' glass transition). If such a transition occurs in a region of the phase diagram where two coexisting crystalline phases are expected, the growth of one phase could be preferentially 'blocked' by the selective nature of

the dynamics in the glass. In such situations ordered states will apparently 'coexist' with amorphous phases. Generally, in situations where the energies of competing ordered structures are very similar (as simulation predicts is the case for hard-sphere mixtures over wide bands of composition), kinetic factors may favour one phase preferentially over other competing structures. Consequently, the crystalline phase observed in an experiment need not be the equilibrium state but rather a metastable state, with a slightly higher free energy, which is simply formed the quickest.

Finally, for completeness, we mention here other related work. It is remarkable that the first examples of colloidal superlattices (AB_2 and AB_{13}) were found by Sanders [12] in native gem opals, solidified crystals of colloidal silica spheres. It was this discovery that led Murray and Sanders to consider the stability of superlattices of hard spheres. Subsequently, Hachisu and Yoshimura [13] observed at least five superlattice structures, including AB_2 and AB_{13}, in mixtures of charge-stabilized colloidal spheres. However, in these pioneering studies neither the interaction between the particles nor the phase behaviour of the mixtures was well characterized. Recently the stability of the AB_2 and AB_{13} phases has been considered theoretically. The results of Xu and Baus [27], based on density functional methods, and Bartlett and van Megen [28], who estimated entropies from free volume calculations, are in reasonable agreement with the simulations discussed here.

2. Summary of experiment and simulation

2.1. *Experiment*

The preparation and characterization of both the particles [29] and the binary suspensions [21] have been described in detail previously; here we give only a brief summary. The particles comprised spherical cores of amorphous PMMA stabilized sterically by thin, 10–15 nm, shells of poly(12-hydroxystearic acid) (PHSA). They were suspended in mixtures of decahydronaphthalene (decalin) and carbon disulphide in a proportion chosen such that the refractive index of the mixture was close to that of the particles ($\sim 1{\cdot}50$). This provided nearly transparent 'index-matched' samples suitable for study by both direct observation and light scattering. A number of previous experiments (see reference [28] for further discussion) on one-component suspensions of this type has established that the interaction between the PMMA particles is well approximated by that of hard spheres.

Suspension concentrations were determined as follows. Several samples of each individual component were prepared over a range of weight fractions which spanned the freezing transition. After the samples had reached equilibrium, the hard-sphere freezing volume fraction, $\phi_F = 0{\cdot}494$, was identified by extrapolating to zero [20, 30] the volume of crystal in samples in the fluid–crystal coexistence region. Then effective hard-sphere volume fractions ϕ, used henceforth, of samples at any known weight concentration could be calculated. This procedure provides an accurate determination of the effective density of the composite PMMA/PHSA particle in the decalin/CS_2 mixture. Since small colloidal particles contain a higher proportion of the low density PHSA shell than larger particles the density of the composite colloid is a slowly increasing function of particle size. The variation is, however, relatively small with densities, defined as the mass of the dry particle divided by the volume in suspension of the composite PMMA/PHSA colloid, determined for the smallest (186 nm) and largest (321 nm) particles of $0{\cdot}979$ and $1{\cdot}008\ g\ cm^{-3}$, respectively.

Mixtures were prepared by combining, in the required proportions, stock solutions of individual components with volume fractions calculated from the experimentally determined composite particle densities. The desired final concentration of a sample was achieved by centrifuging the particles down, removing the clear supernatant, and redispersing the particles by tumbling. Particle number ratios were estimated from the calculated volume fractions of each component in the mixture and the particle radii listed below.

The particle radii were calculated from the lattice parameters of crystals at the melting concentration, measured by light powder crystallography [31]. Particles with radii 186 ± 3, 199 ± 3 and 321 ± 3 nm were used; combination of the first or second with the third provided size ratios of $\alpha = 0{\cdot}58 \pm 0{\cdot}01$ or $\alpha = 0{\cdot}62 \pm 0{\cdot}01$. The polydispersities (standard deviation/mean size) of all species, determined by dynamic light scattering and transmission electron microscopy, were 0·04–0·05.

While one-component PMMA suspensions typically reach their equilibrium states within a day or two of mixing, binary mixtures crystallize much more slowly, sometimes taking weeks or months. Over such long times, sedimentation of the particles under gravity can dominate crystallization, leading to inhomogeneous amorphous sediments. In our experiments the effects of gravitational settling were minimized by rotating the samples continuously but slowly—one revolution per day—in the vertical plane so that the particles experienced 'time-averaged zero gravity' [32]. From time to time they were removed from the rotator for study and then replaced to resume slow rotation.

Crystallization, when observed, appeared to be homogeneously nucleated: small crystallites grew throughout the samples. In partially crystalline samples, the crystallites settled under gravity within a few hours after removal from the rotator, leaving sharp boundaries separating (upper) colloidal fluid phases from (lower) crystalline phases. Since their lattice parameters are comparable in magnitude with the wavelength of visible light, crystallites were visible as coloured specks in white light illumination. Direct observation therefore provided two types of information: first, the phase composition of the sample as fluid, crystalline or a mixture of the two; and second, some measure of the rate at which crystallization takes place. In particular we noted the time after mixing at which crystallites were first observed and the time taken for the sample to reach equilibrium i.e. the time after which the volume of the solid phase no longer changed. Because light scattering and electron microscopy often suggested that the solid portion of these samples contained *both* amorphous and crystalline regions we did not attempt to compare quantitatively the amount of the solid phase with the predictions of the computer simulations.

The structures of the crystals were identified by 'light powder crystallography'. An expanded laser beam illuminated a large number of randomly oriented crystallites; measurement of the scattered light intensity over a range of angles provided 'powder' diffraction patterns. Because the form factors of the individual particles are difficult to determine in index-matched samples [21] we do not attempt to analyse the intensities of the Bragg reflections but identify structures simply from their positions. A few dried samples of the crystalline phases were studied by scanning electron microscopy. Examples of both powder diffraction patterns and electron micrographs are given in [21] and [22].

Before embarking on a detailed comparison of experimental behaviour with that predicted by simulation we will discuss a number of factors which could complicate the situation. A general issue is the extent to which the system studied experimentally

approximates the ideal binary mixture of hard spheres examined in the simulations. We consider first the nature of the interaction between the PMMA particles. In a non-polar medium, electrostatic effects should be negligible while attractive van der Waals forces are expected to be minimized by matching the refractive indices of the particles and suspension medium. Steric stability of closely spaced particles results from the repulsive force induced by compression of their layers of stabilizer. Calculations [21] suggest that the interparticle potential increases from zero when the layers are just in contact to $\sim 10k_BT$ on a decrease of 2–3 nm of the interparticle spacing. Thus the potential, while continuous, is extremely steep; for particles of diameter $\geqslant 400$ nm in Brownian motion, the potential increases from zero to essentially infinity when the interparticle spacing changes by less than 0·5%. Experiments [28] on the phase behaviour, structure and dynamics of PMMA suspensions, as well as measurements of osmotic pressure [33], support these theoretical estimates. Therefore we do not expect the inevitable slight softness of the particles to be a significant complicating factor.

A second concern is that PMMA particles of any one species have a distribution of size. It is known both theoretically [18] and experimentally that a polydispersity of $\geqslant 0{\cdot}08$ suppresses crystallization of a one-component hard-sphere system by distortion of the putative lattice. However, there is as yet no experimental evidence that the smaller polydispersities, 0·04–0·05, typical of the particles used in this work seriously affect either the freezing transition or the structure of the crystals. It remains possible that this degree of polydispersity has a greater effect in binary mixtures; however, lacking direct evidence, we cannot explore this possibility further.

Another factor which must be considered is the reliability of the volume fractions assigned to the experimental samples. We estimate that the sample preparation procedure outlined above could result in uncertainties in the total volume fraction of order 0·01. Furthermore the concentrations of the samples could change somewhat during the many months over which they were observed. Periodic weighing revealed occasional minor loss of liquid by evaporation, despite careful sealing of the sample cells. It is known that carbon disulphide penetrates and swells the particles to some extent [34]. The process is fairly rapid and occurs largely within the first few hours after exposure of the particles to carbon disulphide; it is allowed for in the sample preparation procedures outlined here. However, further penetration may occur over a longer time. These uncertainties must be borne in mind when attempting quantitative comparisons.

2.2. *Simulation methods*

2.2.1. *Free energy data*

In order to compute the phase diagram by simulation methods we require the equations of state and free energies of all competing phases. As discussed in the introduction, the possible binary solid phases may be identified as those whose density at close packing is similar to that of a one-component f.c.c. crystal of hard spheres. From this criterion, the possible solid phases are the pure solids, AB_2 and AB_{13}.

The free energies were obtained using thermodynamic integration methods. For the binary fluid, we compute the work needed to compress the fluid mixture from zero density (the ideal gas) to the required packing fraction. The semi-empirical equation of state of Mansoori *et al.* [35] was used for this purpose since test calculations [17] for several compositions and size ratios, $0{\cdot}50 \leqslant \alpha \leqslant 0{\cdot}60$, have

shown that it introduces negligible errors up to packing fractions of order 0·55, which is sufficiently high for our purposes. The reliability of the Mansoori equation was confirmed previously by Jackson *et al.* [36] for smaller size ratios.

For the solid state free energies we made use of the Frenkel–Ladd method [6], in which the reference state is taken to be the corresponding Einstein crystal. These calculations have been described in detail elsewhere [24, 25]. For the pure solid A, the equation of state agreed well with that of Young and Alder [5], who provided a convenient polynomial representation. We have presented similar expressions for the AB_{13} and AB_2 free energies in [24] and [25]. A full set of pressures and free energies is given in [17].

2.2.2. *Phase diagrams*

The (ϕ_A, ϕ_B) constant volume phase diagrams were calculated from the free energy data in two stages. First, the equilibrium conditions were applied at constant pressure, using 'common-tangent construction' [37, 38] to characterize the coexisting phases and construct a constant pressure phase diagram. To convert the pressure–composition phase diagrams into the (ϕ_A, ϕ_B) representation the calculated tie lines at each pressure are considered. The equation of state for each of the coexisting phases is inverted to find the appropriate packing fraction and the equivalent tie line in the (ϕ_A, ϕ_B) representation is constructed. In this way the phase boundaries in the (ϕ_A, ϕ_B) plots are located.

Errorrs in the phase boundaries stem from three sources. The statistical errors in the solid-state free energies are the most easily quantified. These are typically around $0{\cdot}01 k_B T$ per particle. To obtain interpolated free energies at packing fractions between those at which simulations were made, a fit to the equation of state is integrated. For the calculations presented here, simple polynomial fits for the excess free energy F_{ex} at a single value of the size ratio were used, rather than the global (ϕ, α) fits given in [24] and [25]. These were very accurate, and the errors in the interpolated free energies are not expected to be significantly larger than the statistical errors in the values calculated explicitly.

In recent years finite size problems have been treated with increasing care. Here no attempt has been made to correct for the limited size of the simulations carried out. 896 particles were used in the AB_{13} simulations and 648 in the AB_2 ones. However, previous analyses of the finite size problem for free energies calculated by the lattice-coupling method [6] revealed corrections that are smaller than the statistical errors quoted in this work.

A second source of error lies in the fluid-state free energy and particularly in the reliability of the Mansoori equation of state [35]. The Mansoori equation has been tested extensively by Jackson *et al.* [36] and in this work over the range of α of interest. It is generally believed to be accurate for densities where solid–fluid phase coexistence has been calculated. Although some systematic error may be anticipated from this source, it is likely to be of the same order of magnitude as the (random) statistical error of the solid-state free energies. We demonstrate the potential significance of this error below.

A third possible source of error comes from finding the point of contact of the common tangent to the fluid curve. However, since the Mansoori equation is a smooth function it is expected that the errors associated purely with finding the tangent to the fluid curve that passes through a solid free energy point are very small,

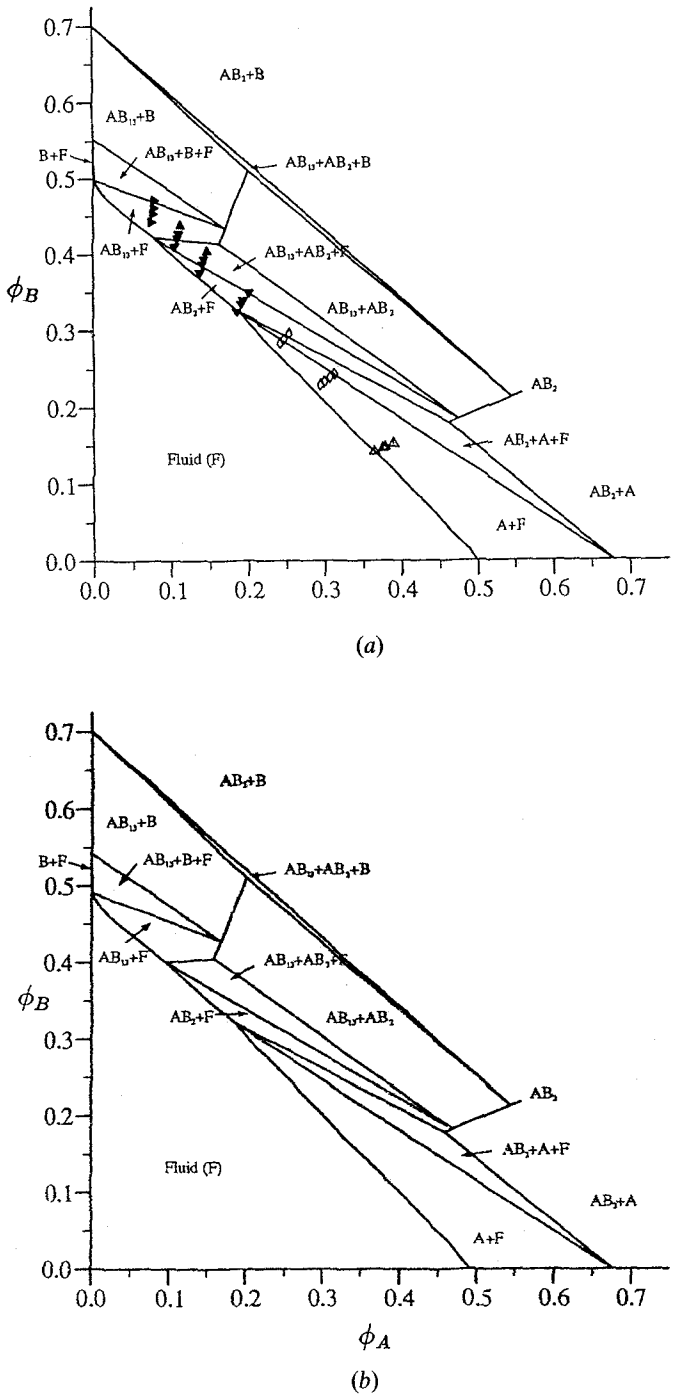

Figure 1. (*a*) Phase diagram at constant volume of a binary mixture of hard spheres with a diameter ratio $\alpha = 0{\cdot}58$. In addition to the fluid phase F, the following stable solid phases appear: pure A, pure B, AB_2 and AB_{13}. Also shown are the state points studied by Bartlett *et al.* [22] in colloidal suspensions: ▶, AB_{13} + B + F; ▼, AB_{13} + F; ▲, AB_{13}; ◇, AB_2 + F; △, amorphous solid. (*b*) The effect on the $\alpha = 0{\cdot}58$ phase diagram of increasing the free energy of the fluid by $0{\cdot}1k_BT$.

i.e. a much smaller effect than that caused by the statistical errors in the solid-state free energies.

In order to indicate the insensitivity of the phase diagrams (in the location of phase boundaries) to systematic errors of the size estimated, a simple shift has been applied to the fluid free energies and the diagram recalculated. Figure 1(*b*) shows the resulting phase diagram with the fluid free energy surface artificially raised by $0{\cdot}1k_BT$ per particle. This value is approximately ten times the average statistical error in the solid-state free energies. Figure 1(*a*) shows the original diagram for comparison. Overlaying the two figures reveals only marginal differences in the phase boundaries and indicates a striking insensitivity to such a large perturbation. The solid–fluid phase boundaries shift to slightly lower densities as expected and the most noticeable changes are in the AB_{13} + F and AB_{13} + AB_2 + F regions.

3. Simulation phase diagrams for $0{\cdot}50 \leqslant \alpha \leqslant 0{\cdot}625$

The results of computer simulation are most conveniently compared with experiment by portraying the calculated phase diagram in the (ϕ_A, ϕ_B) plane. In this representation mixtures of constant composition lie along rays which radiate from the origin at a fixed polar angle, while the radial distance labels the total volume fraction $\phi_A + \phi_B$. The phase rule dictates that for a binary mixture of hard spheres the maximum number of coexisting phases is three, so the (ϕ_A, ϕ_B) plane is divided into regions of one-, two- and three-phase coexistence. Figure 1(*a*) shows a few examples of the calculated tie-lines which in areas of two-phase coexistence connect the equilibrium phases. The proportion of each equilibrium phase is given by the standard lever-rule construction. In the three-phase regions the vertices of the bounding triangle label the densities and compositions of the three coexisting phases while the proportions of each phase are given by a simple geometric construction [26]. Phase diagrams were calculated for size ratios ranging from 0·5 to 0·625. Figure 2 shows the range $0{\cdot}5 \leqslant \alpha \leqslant 0{\cdot}59$ and figure 3 the range $0{\cdot}60 \leqslant \alpha \leqslant 0{\cdot}625$.

Based on their experimental observations at $\alpha = 0{\cdot}58$, Bartlett *et al.* [22] proposed what is probably the simplest possible form of the (ϕ_A, ϕ_B) phase diagram for a binary mixture with four crystalline states, A, B, AB_2 and AB_{13}. With increasing particle concentration, the following phase behaviour was suggested (see figure 1, reference [22]): fluid for all compositions; four two-phase regions, each comprising fluid and one of the crystals; three eutectic triangles A + AB_2 + fluid, AB_2 + AB_{13} + fluid and AB_{13} + B + fluid; and, at the highest concentrations, crystal–crystal coexistence, A + AB_2, AB_2 + AB_{13} and AB_{13} + B. In fact the phase diagram for $\alpha = 0{\cdot}58$ (figure 1(*a*)) calculated subsequently in the simulations [25] looks, at a first glance, to be considerably more complicated. However, a detailed comparison with the phase diagram suggested by Bartlett *et al.* [22] shows some striking similarities. Both diagrams contain the same combinations of phase coexistences; all that is altered is their relative disposition in the plane. Indeed the calculated phase diagram (figure 1(*a*)) is simply a severely distorted form of the earlier diagram suggested by Bartlett *et al.* This can be seen by focusing on the positions of the three eutectic fluid compositions (where a fluid phase coexists with crystals of either A + AB_2, AB_2 + AB_{13} or AB_{13} + B). In the calculated phase diagram these three points, and their associated phase boundaries, are skewed towards the small sphere (Y) axis when compared with the earlier phase diagram of Bartlett *et al.*

The underlying reason for this asymmetry is that the osmotic pressure is increasing

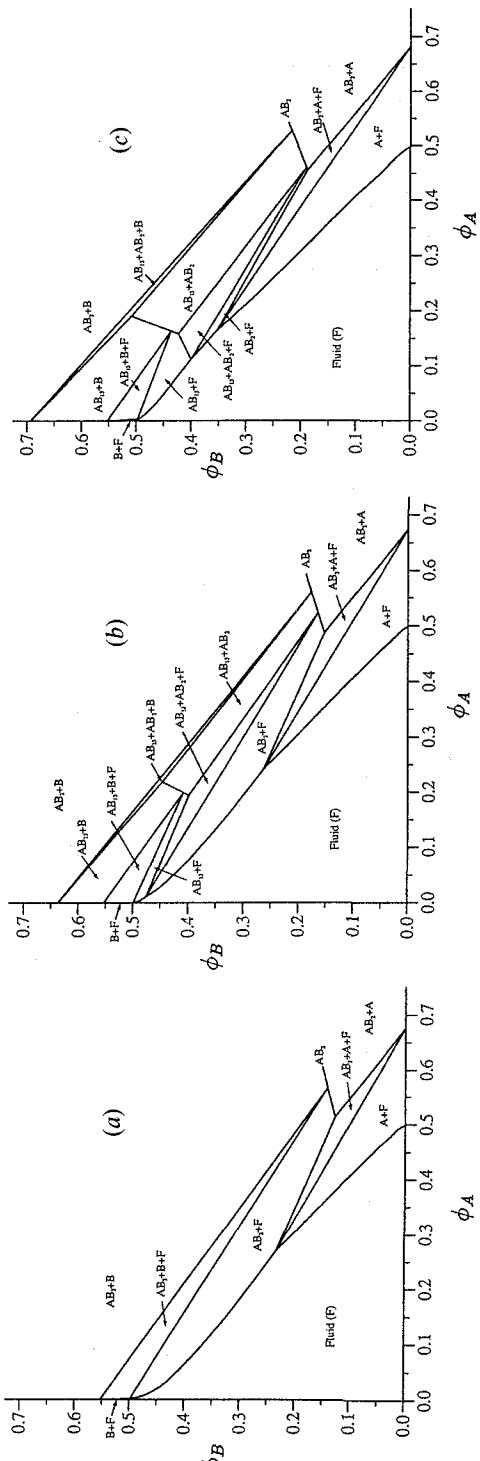

Figure 2. The calculated equilibrium phase diagrams at radius ratios (*a*) $\alpha = 0{\cdot}50$, (*b*) $\alpha = 0{\cdot}54$ and (*c*) $\alpha = 0{\cdot}59$.

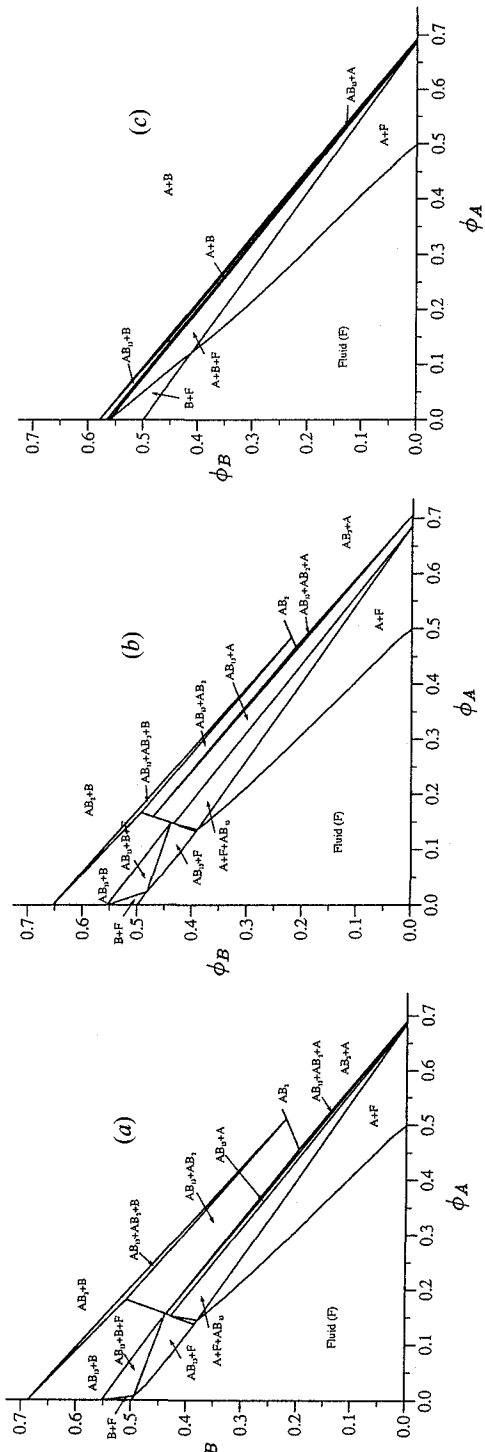

Figure 3. The calculated equilibrium phase diagrams at radius ratios (*a*) $\alpha = 0{\cdot}60$, (*b*) $\alpha = 0{\cdot}61$ and (*c*) $\alpha = 0{\cdot}625$.

at fixed total ϕ across the diagram. At the freezing points of the pure solids (i.e. at $(\phi_A, \phi_B) = (0, 0{\cdot}494), (0{\cdot}494, 0)$) the pressures are in the ratio of number densities (i.e. α^3). To illustrate the consequence of this consider a sample of equal volume fractions ($\phi_A = \phi_B$) at $\alpha = 0{\cdot}625$ (figure 3(*c*)); this corresponds to a composition of $n_B/n_A = 4$ which, given the preponderance of B particles, might be expected to crystallize out pure B above the freezing density. In fact, as the diagram shows, crystallization into a highly compressed A occurs, leaving a fluid enriched in B at a lower density than the mean. The dominant factor contributing to the lowering of the free energy of the sample upon crystallization is the increased free volume available to the larger number of small particles in the lower density fluid.

First we discuss the predicted diagrams for $0{\cdot}5 \leqslant \alpha \leqslant 0{\cdot}59$ (figure 2). The diagrams are generically similar, showing the behaviour described earlier: four two-phase fluid–crystal coexistence regions, three three-phase eutectic triangles and three regions of crystal–crystal coexistence. (Since the experimental results do not extend to very high concentrations the three-phase crystal region B + AB_2 + AB_{13} does not concern us here.) However, the position and extent of each region are strong functions of the size ratio α. Two features are striking: (i) the large extent of the A + fluid region, and thus even at number ratio $n_B/n_A = 6$, a fluid is predicted to freeze first into A + fluid rather than AB_2 + fluid or AB_{13} plus fluid, as one might expect naïvely; (ii) the fact that the AB_2 + fluid region extends to very large values of n_B/n_A so that at $\alpha = 0{\cdot}54$ a fluid mixture with $n_B/n_A \simeq 50$ should freeze first into AB_2 + fluid rather than AB_{13} + fluid. Even at $\alpha = 0{\cdot}58$, where experiments were performed, a fluid at $n_B/n_A = 13$ is predicted to form AB_2 + fluid rather than AB_{13} + fluid.

Between $\alpha = 0{\cdot}59$ (figure 2(*c*)) and $\alpha = 0{\cdot}60$ (figure 3(*a*)) a qualitative change in the form of the diagrams is found. The AB_2 + fluid, AB_2 + AB_{13} + fluid, and AB_2 + A + fluid regions disappear, so that AB_2 should be found only at very high concentrations. A fluid + AB_{13} + A triangle appears. Again, the predicted phase behaviour is a strong function of size ratio. At $\alpha = 0{\cdot}62$ AB_2 is found only at the highest concentrations, and at $\alpha = 0{\cdot}625$ AB_{13} also has almost disappeared. As we shall see in the next section, the sensitivity of the phase behaviour for radius ratios $\alpha \simeq 0{\cdot}62$ has important consequences when we compare the results of computer simulations with experiment. For $\alpha > 0{\cdot}625$ the phase diagram is expected to take the simple form predicted by Bartlett [26], corresponding to an A–B eutectic. This should hold up to $\alpha \simeq 0{\cdot}85$ above which, because of their increasingly similar sizes, mixed, substitutionally disordered crystals of A and B become possible.

Finally we note that at the very highest packing fractions, $\phi \sim 0{\cdot}65$, all the calculated phase diagrams demonstrate that the most stable solid phases are those predicted by Murray and Sanders [11]. Thus at $n_B/n_A \simeq 2$ solid AB_2 is stable; at $n_B/n_A \simeq 13$, AB_{13} is stable, and at number ratios intermediate between the ideal stoichiometries, phase separation into the two adjoining solid phases is predicted.

4. Comparison of experiment and simulation

4.1. *Radius ratio* $\alpha = 0{\cdot}62$

The samples prepared at $\alpha = 0{\cdot}62$ are plotted on the phase diagram, figure 4, predicted by simulation. We show both samples which have been discussed previously [21] and some new ones at $n_B/n_A \sim 2$, 4, 10 and 13. Here, for completeness, we summarize the behaviour of all samples. We note that the total volume fractions are

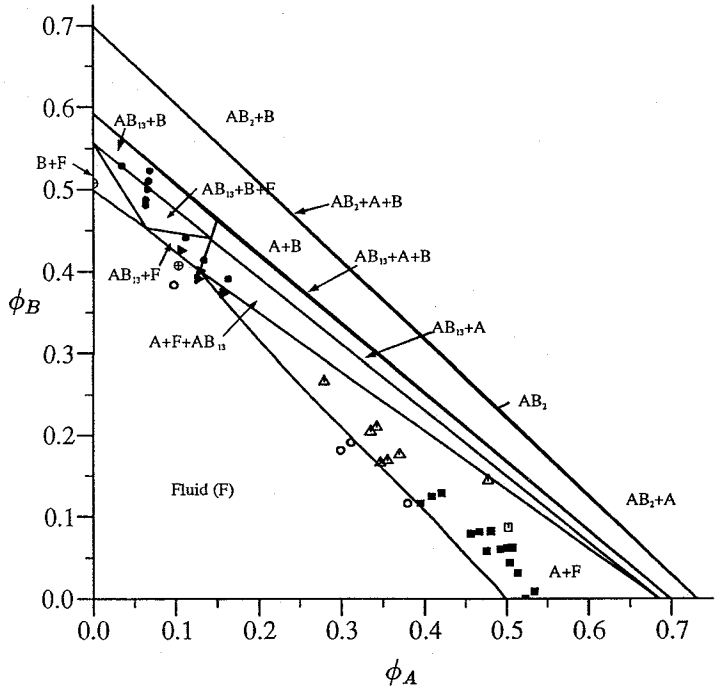

Figure 4. Phase diagram at constant volume of a binary mixture of hard spheres with a diameter ratio $\alpha = 0{\cdot}62$. The symbols indicate that the following phases were detected by Bartlett *et al.* [21] in colloidal suspensions: ○, Fluid (F); △, amorphous solid; ●, B; ▶, AB_{13} + B + F; ⊕, B + F; ■, A + F; □, A.

mostly in the range $0{\cdot}49 < (\phi_A + \phi_B) < 0{\cdot}56$, which covers the coexistence region of a one-component system where crystallization is fairly rapid. By analogy with the one-component system, we expected that more concentrated samples would tend to remain in metastable glassy states; however, this remains to be established at all number ratios. Samples rich in A, $0 \leqslant n_B/n_A \lesssim 1{\cdot}2$, formed crystals of essentially pure A coexisting with fluid enriched in B. The time taken for the samples to reach their equilibrium coexistence states increased rapidly with increasing content of B, from the day or so characteristic of a one-component A sample to many weeks. This slowing down presumably reflects the ejection of an increasing number of small B particles from the growing A crystals. For $1{\cdot}2 \leqslant n_B/n_A \lesssim 4$ no crystallization was observed and the samples remained in metastable fluid or glassy states. From figure 4 we note that all samples with $n_B/n_A \sim 4$ are predicted to lie in the A + fluid region. Apart from the tendency to form glasses at large n_B/n_A ratios (which will be discussed further in section 5.1) there is general agreement between experiment and simulation in this region of the phase diagram.

In the opposite limit, samples rich in B, $n_B/n_A \gtrsim 30$, formed either B + fluid or apparently pure B crystal without fluid. Since there were particles of A in these samples, we must assume that these were trapped in the B polycrystal, probably in amorphous grain boundaries; scanning electron microscopy supports this conjecture [21]. Again there was a marked slowing down of the rate of crystallization with increasing content of the minority (A) species. Figure 4 shows that most of these

samples are predicted to lie in the AB_{13} + B + fluid or AB_{13} + B regions, in disagreement with the fact that AB_{13} was not observed experimentally. However, in figure 3(*c*), for $\alpha = 0{\cdot}625$, we note that these samples lie mainly in the corner of the A + B + fluid triangle where the predominant phase will be crystalline B. Thus given the experimental uncertainty in the diameter ratio ($\alpha = 0{\cdot}62 \pm 0{\cdot}01$) and the difficulty, noted above, in nucleating crystals of A from fluids containing mostly small spheres, there is a reasonable level of agreement between experiment and simulation. Overall the experimental results confirm the prediction from simulation that the size ratio $\alpha = 0{\cdot}62$ is at the upper limit for the stability of both AB_2 and AB_{13}. The former was not observed and the latter, though found, appeared to be metastable.

The most interesting behaviour was observed in samples with $10 \lesssim n_B/n_A \lesssim 16$. The most concentrated of these samples formed apparently pure B crystals (again presumably with trapped amorphous A). At slightly lower concentrations samples containing AB_{13} + B + fluid were found. However, the following observations on a sample with $n_B/n_A = 12{\cdot}9$ and $\phi = 0{\cdot}533$ suggest that the AB_{13} phase may be metastable. Crystallites were first observed in this sample after one day, and after two weeks the fraction of the sample which appeared crystalline remained constant at $0{\cdot}80 \pm 0{\cdot}05$ for the next nine months. Analysis of the powder diffraction patterns, figure 5(*a*) shows that the crystal, when first formed, was essentially pure B (a random-stacked, close-packed structure [31]). After a period of three months, features appeared in the pattern characteristic of the AB_{13} structure. As can be seen from figure 5(*b*), the superlattice reflections are superimposed on a relatively large featureless background. This suggests that the sample contains both crystalline B and AB_{13} phases as well as an appreciable amount of a third disordered phase. Over still longer times, the amount of AB_{13} appeared to decrease, leaving the B crystal, figure 5(*c*, *d*). Because the measurements shown in figure 5 spanned many months, the intensities measured on different occasions are on different arbitrary scales, so the proportions of each of the three phases are difficult to estimate accurately. However, the change in the *relative* amounts of the two crystalline phases may be followed by ratioing the intensity of one of the AB_{13} superlattice reflections, for example the (422) line, to the intense (001) reflection of the randomly stacked B crystal. Figure 6 displays the ratio of these two peaks for measurements at $\lambda = 647{\cdot}1$ nm where the reflections are well separated. As shown, the relative amount of the AB_{13} phase reaches a peak after about six months and subsequently drops, strongly suggesting that the AB_{13} phase is metastable, with respect to B crystal and fluid. The subsequent disappearance of the superlattice phase is, however, very slow with crystallites of AB_{13} remaining visible even a year after sample preparation. Unfortunately, over this long time period the intensity of light scattered by big and small particle changes (probably caused by a small degree of selective evaporation of carbon disulphide from the suspension medium), so we cannot be sure that the metastable AB_{13} crystal grows from B particles trapped in amorphous states, although this seems the most likely explanation.

The behaviour of these samples is not consistent with the predictions of figure 4, for $\alpha = 0{\cdot}62$, that they should lie in the AB_{13} + fluid, A + AB_{13} + fluid or A + fluid regions nor with those of figure 3(*c*), for $\alpha = 0{\cdot}625$, where AB_{13} is only predicted at high concentration. We note, however, that in figure 3(*c*) all the experimental samples lie in or close to regions where B crystals are predicted. Comparing figures 3(*c*) and 4, it is immediately apparent that the equilibrium phase diagrams are very

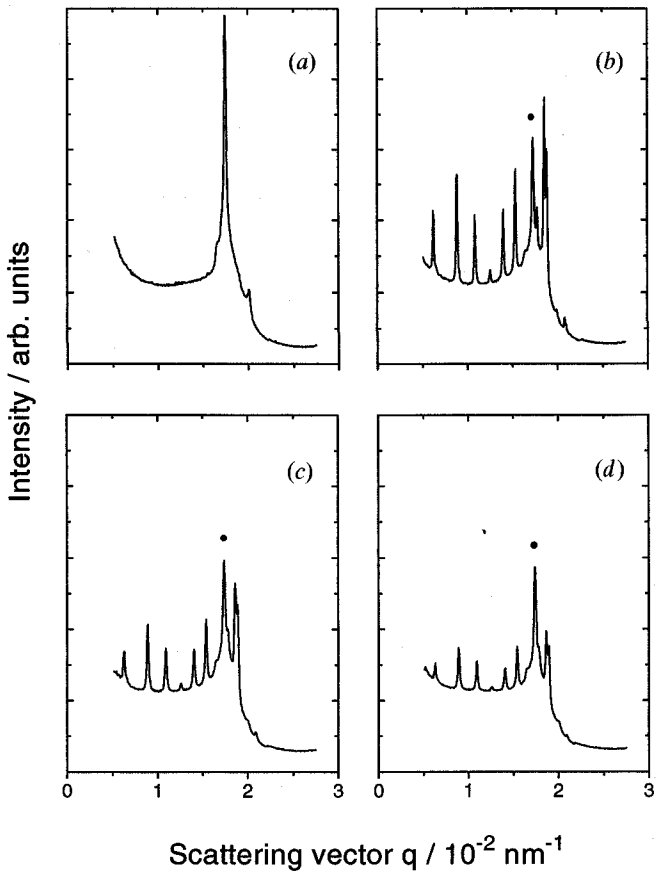

Figure 5. Light scattering diffraction patterns measured for a colloid mixture of radius ratio $\alpha = 0{\cdot}62$, composition $n_B/n_A = 12{\cdot}9$ and volume fraction $\phi_A + \phi_B = 0{\cdot}533$ after (*a*) three, (*b*) six, (*c*) nine and (*d*) twelve months. The dominant Bragg reflection in (*a*) and the marked peaks (●) in (*b–d*) arise from the (001) interplane spacing of a crystal of small spheres. The additional peaks, clearly visible in (*b*), indicate the presence of an AB_{13} phase.

sensitive to small changes in diameter ratio; in particular, note the destabilization of the AB_{13} phase at $\alpha = 0{\cdot}625$ compared with the case at $\alpha = 0{\cdot}62$ and the subsequent marked change in the phase equilibria for compositions around $n_B/n_A = 13$. This sensitivity reflects the very similar free energies of the competing crystalline phases. In this situation we can expect kinetic factors to play a dominant role in determining which phases are found experimentally. The surprising observation of *metastable* AB_{13} must therefore indicate that this phase is formed more readily than the thermodynamically preferred B crystal. Possible explanations for this kinetic effect are discussed in section 5.2. However, the apparent readiness of AB_{13} to nucleate does not explain fully the complex sequence of phase behaviour observed in the experiments. The scattering data show clearly that the thermodynamically stable B crystal nucleates first and only later does the metastable AB_{13} grow. The explanation of why a metastable phase should appear at all if a more stable phase has already nucleated remains unclear.

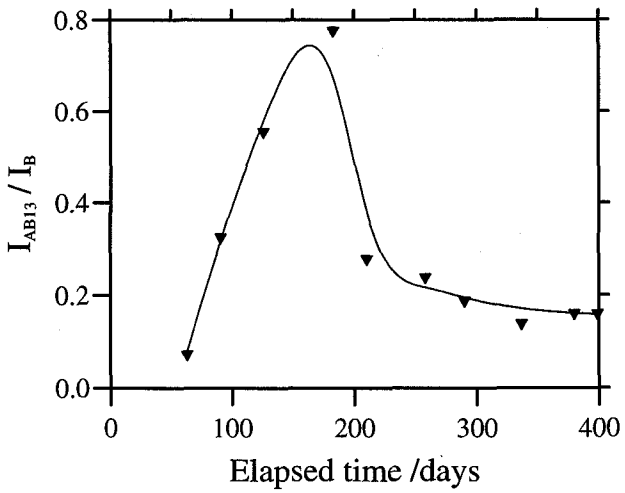

Figure 6. The ratio of the light scattering intensities of the AB_{13} (422) line ($I_{AB_{13}}$) to the B (001) line (I_B) as a function of time after preparation, for a colloidal sample of radius ratio $\alpha = 0{\cdot}62$, $n_B/n_A = 12{\cdot}9$ and $\phi = 0{\cdot}533$.

4.2. *Radius ratio* $\alpha = 0{\cdot}58$

The samples prepared at $\alpha = 0{\cdot}58$ are plotted on the phase diagram, figure 1(*a*) predicted by simulation. Because we expected mixtures with $n_B/n_A \lesssim 1{\cdot}2$ to behave in much the same way as at $\alpha = 0{\cdot}62$, i.e., to form A crystal + fluid, no such samples were prepared. A surprising finding, initially, was that the samples at $n_B/n_A = 2$, corresponding to the stoichiometry of AB_2, did not crystallize. Subsequent simulations showed that these samples are predicted to lie in the crystal A + fluid region, where amorphous structures were also found at $\alpha = 0{\cdot}62$. It remains to be established whether, as predicted in figure 1(*a*), samples of this composition but higher total concentration would form AB_2 or whether crystallization would be superseded by a glass transition.

In all the samples at both $n_B/n_A = 4$ and $n_B/n_A = 6$ the final state was AB_2 + fluid, with differing proportions of the two phases. This crystal structure was clearly identified from both the light scattering diffraction patterns and electron microscopy of dried samples [22]; the electron micrographs showed beautiful long-range binary order. In all cases crystallization was slow. The first crystallites were observed within 4–5 weeks and full crystallization took at least three months. Figure 1(*a*) shows that samples at $n_B/n_A = 6$ are predicted to lie either in the AB_2 + fluid region or near to the corner of the AB_2 + A + fluid region. If we assume that A remains amorphous there is reasonable agreement between experiment and simulation. However, the situation is less satisfactory for the samples at $n_B/n_A = 4$ which showed AB_2 + fluid experimentally but are predicted to be mainly in the A + fluid region. Possible explanations for this behaviour are discussed in section 5. Points of good agreement concern the total concentration of the AB_2 crystal and the hexagonal interlayer-spacing or c/a ratio. Experimentally, these parameters were calculated from the measured lattice constants of the crystal and the known particle sizes. The volume fraction of AB_2, in the samples in which it was observed, was between 0·63 and 0·65 whereas the lowest predicted value is $\sim 0{\cdot}64$. There was a similar degree of agreement

for the c/a ratio with an experimental value of $1{\cdot}045 \pm 0{\cdot}002$, for samples at $n_B/n_A = 4$, against a computed value of 1·049.

The most concentrated sample at $n_B/n_A = 14$ and 20 appeared to be entirely AB_{13} but presumably contained some solid B, either in an amorphous state or as a crystal which would be hard to identify (see discussion below). The other samples at $n_B/n_A = 14$ and 20, and those at $n_B/n_A = 9$ showed AB_{13} + fluid coexistence. The AB_{13} structure was indicated clearly by light crystallography; the appearance of superlattice lines in the diffraction patterns confirmed the presence of the large unit cell described in section 1. Electron microscopy of dried AB_{13} was not very successful, probably because of disruption of the crystal on drying. Surprisingly, AB_{13}, despite its complex structure, crystallized much more rapidly than AB_2. At $n_B/n_A = 20{\cdot}0$ and $\phi_A + \phi_B = 0{\cdot}538$ crystallites were observed within three days and complete crystallization took about three weeks. Inspection of figure 1(*a*) shows that at $n_B/n_A = 20$ most of the samples lie in the AB_{13} + fluid region, in agreement with the observations. At $n_B/n_A = 14$ most samples are predicted to show three-phase AB_{13} + AB_2 + fluid coexistence, whereas AB_{13} + fluid was observed. There is consistency if we assume that the AB_2 remains amorphous. Samples at $n_B/n_A = 9$ show the most serious disagreement with predictions: AB_2 + fluid is predicted whereas AB_{13} + fluid is seen. This behaviour is discussed further in section 5. As measurements on the AB_2 crystal demonstrated there is a good agreement between observed and predicted values for the concentration of superlattice phases. For all the samples discussed in this paragraph the total volume fraction of AB_{13} lay in the range 0·58–0·60, whereas the lowest value predicted by simulation is about 0·58.

In all the samples prepared at $n_B/n_A = 30$ fluid–solid coexistence was observed, with crystals of AB_{13} being clearly identifiable from light crystallography. Simulation predicts that while the three most dilute samples lie in the AB_{13} + fluid region the remaining sample should show a three-phase coexistence between AB_{13}, B, and fluid. Checking this prediction is difficult experimentally because at a diameter ratio of $\alpha = 0{\cdot}58$ there is a near overlap of the main peak of the B crystal with one of the AB_{13} lines. Close inspection of the light scattering diffraction patterns does, however, reveal several features which while not conclusive are consistent with the theoretical predictions. Figure 7(*a–d*) shows the measured scattering from samples with $n_B/n_A = 30$ and $\phi_A + \phi_B = 0{\cdot}520$, 0·533, 0·542 and 0·553. Concentrating on the two peaks at $1{\cdot}9 \times 10^{-3}$ and $2{\cdot}0 \times 10^{-2}$ nm^{-1} we can clearly see there is a change in their relative intensity between parts (*a–c*) and part (*d*). The peak at $2{\cdot}0 \times 10^{-2}$ nm^{-1} arises from the very intense (531) reflection [22] of the AB_{13} crystal while the peak at $1{\cdot}9 \times 10^{-2}$ nm^{-1} may arise from either the strong (001) reflection of the B crystal (if present) or the (440) line of AB_{13}. Under the index-matching conditions used in the experiments at $\lambda = 476{\cdot}2$ nm the (440) line of AB_{13} is normally found to be significantly weaker than the strong (531) peak, as is indeed observed in figure 7(*a–c*). The reversal of the intensity ratio in figure 7(*d*) therefore indicates that the most concentrated sample contains both AB_{13} and B crystals, as predicted.

5. Structural and thermodynamic effects on crystallization kinetics

If one accepts at face value the comparison of phases observed experimentally in the suspensions with those predicted from the hard-sphere thermodynamic phase diagram, some aspects about the kinetic factors influencing which crystalline phases are observed experimentally may be inferred.

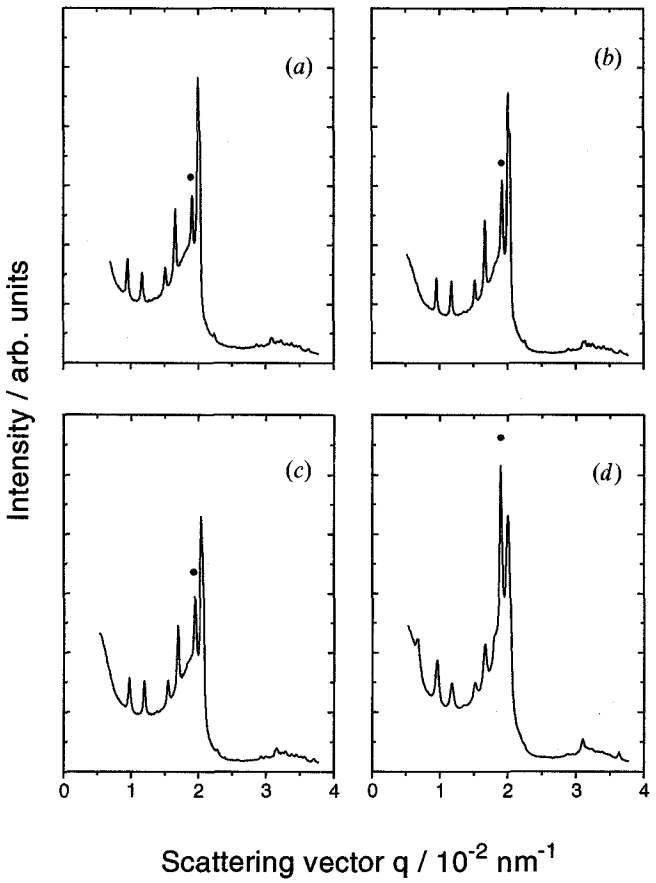

Figure 7. The measured light scattering from colloidal samples of radius ratio $\alpha = 0{\cdot}58$ with $n_B/n_A = 30$ and (*a*) $\phi_A + \phi_B = 0{\cdot}520$, (*b*) 0·533, (*c*) 0·542 and (*d*) 0·553. The marked peak (●) at $q = 1{\cdot}9 \times 10^{-2}$ nm^{-1} may arise from either the (001) interplane reflection of a crystal of small spheres or the (440) line of an AB_{13} crystal. The two lines are almost coincident. The remaining peaks indicate the presence of an AB_{13} crystal.

Two general features emerge from this comparison. First, AB_{13} seems to crystallize very readily out of the suspensions. In contrast to the other crystalline phases, it is detected experimentally whenever it is predicted on thermodynamic grounds, and even, in some cases, at compositions where other phases are expected to be more stable. Second, pure A and AB_2 seem reluctant to crystallize out of suspensions whose compositions differ substantially from those of the crystals. The thermodynamic phase diagrams show that at both $\alpha = 0{\cdot}58$ and $\alpha = 0{\cdot}62$ solid A should precipitate out of fluids with a wide range of compositions, from pure A to $n_B/n_A \sim 9$. Experimentally, as seen in figure 4, pure A appears only from suspensions of composition $n_B/n_A \lesssim 1{\cdot}2$, for $\alpha = 0{\cdot}62$; for larger n_B/n_A values an amorphous solid is found. Similarly, for $\alpha = 0{\cdot}58$ (figure 1(*a*)), amorphization occurs at composition $n_B/n_A = 2$ whereas at $n_B/n_A = 4$ solid AB_2 appears rather than A, as would be expected from the thermodynamic phase diagram.

In the $n_B/n_A = 4$ mixture ($\alpha = 0{\cdot}58$), it is as if the system has settled into the next

most stable state in order to avoid crystallizing A from the B-rich fluid. Similarly, for fluids of composition $n_B/n_A = 9$, AB_{13} appears, rather than AB_2, as expected on thermodynamic grounds. In order to make this observation more concrete, we have recalculated phase diagrams at $\alpha = 0{\cdot}58$ with the A and AB_2 crystals artificially destabilized with respect to the other phases. By *thermodynamically* destabilizing these crystals, we are attempting to explore the consequence of formation of these phases being blocked *kinetically*, and to expose the boundaries between the fluid and the underlying metastable phase. In figure 8(*a*) we show the phase boundaries calculated

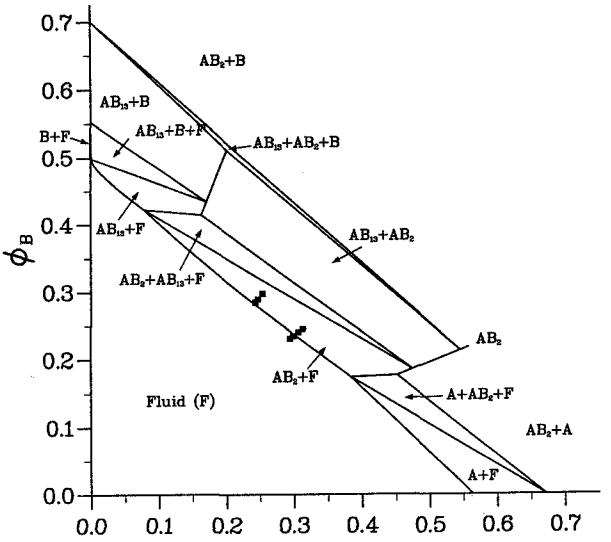

(*a*)

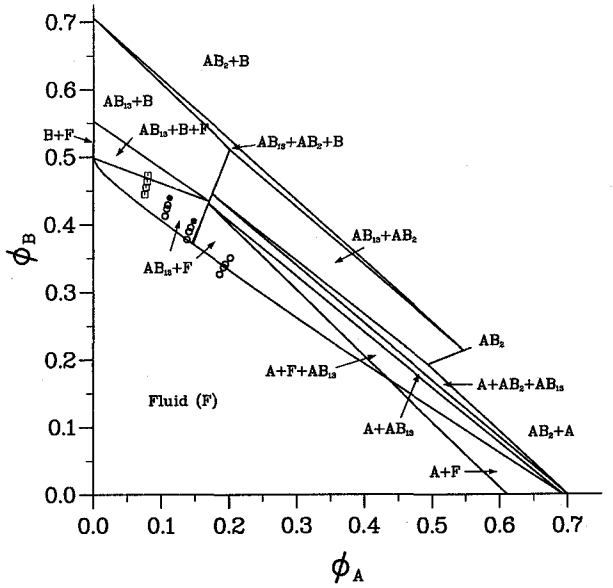

(*b*)

Figure 8. The effect on the phase diagram for $\alpha = 0{\cdot}58$, shown in figure 1(*a*), of (*a*) an increase in the free energy of solid A by $k_B T$ and (*b*) an increase in the free energies of both solids A and AB_2 by $k_B T$. The experimentally observed phases are indicated as in figure 1.

by artificially raising the free energy of solid A by k_BT. These locate possible transitions to metastable phases accessible to suspensions with composition $n_B/n_A = 4$ as they are compressed, if nucleation of crystalline A is blocked because of the large difference between the composition of fluid and solid. The points examined experimentally at these compositions are also shown. It can be seen that all the experimental points at which solid AB_2 was found now lie in or very close to the metastable two-phase region of AB_2 + fluid.

In order to examine the same trends for the very B-rich suspensions, where nucleation of both A and AB_2 could be blocked, we show in figure 8(*b*) the effect of destabilizing both A and AB_2 by k_BT. Again, experimental points which lay previously in a region of predicted stability for fluid plus A and AB_2 ($n_B/n_A = 9$), but where AB_{13} was observed, are now located in, or very close to, an AB_{13} + fluid region.

These considerations lend substance to the idea that the experimental observations are affected by kinetic effects. In the following sections we describe preliminary attempts to identify factors which might lead the kinetics of crystallization to depend on the composition of solid and melt.

5.1. *Fluid composition and crystal nucleation*

The experimental observations on the binary crystals are consistent with the formation of crystals by a process of homogeneous nucleation. Careful observations have been made on the kinetics of crystal formation in the one-component hard-sphere colloids [39]. Homogeneous nucleation is observed for packing fractions below $\phi = 0{\cdot}58$ (which is the density at which diffusion is arrested). At higher densities, heterogeneous nucleation is seen, which results in distinctively textured crystals growing away from interfaces.

We have investigated some possible reasons for a relationship between ease of crystallization and the difference in composition between crystal and fluid by calculating some of the parameters which appear in classical nucleation theory as applied to crystallization of solid A from a binary mixture.

In classical theory, the rate of homogeneous nucleation is expressed as the product of a thermodynamic factor, which gives the number of nuclei which have reached a critical size N_s^*, and a kinetic factor f^*, which governs the rate at which further A particles are added to the critical nucleus:

$$J_{\text{nucl}} = f^* N_s^*. \tag{1}$$

Both of these factors depend on the mole fraction of A particles in the fluid X_A. The kinetic factor f^* contains a trivial factor proportional to X_A, which arises from the proportion of fluid atoms around the surface of the critical nucleus which are of type A and may therefore stick on, and a potentially complicated X_A dependence from the rate at which the rearrangement necessary to include one of the fluid atoms into the crystal takes place. We have not investigated the composition dependence of the latter factor here; instead we have simply set it to be proportional to the diffusion coefficient of a one-component hard-sphere fluid with the same total packing fraction [7].

Nucleation theory is normally developed at constant pressure, where the number of critical nuclei (per unit volume) that have reached the critical size N_s^* will be

$$N_s^* = N_0 \exp\left(-\frac{\Delta G^*}{k_B T}\right). \tag{2}$$

Here, the liquid contains N_0 A atoms per unit volume, and ΔG^* is the Gibbs free energy of formation of the critical nucleus (presumed spherical). The colloidal experiments are carried out at constant volume, so that the thermodynamic driving force is really the change in the Helmholtz free energy of the whole sample when a crystal nucleus forms. However, since the crystal nucleus is at the same osmotic pressure as the liquid, it is easy to show that, for the formation of a nucleus which is very small compared with the whole sample, the difference between these free energies is insignificant.

ΔG^* is given by

$$\Delta G^* = \frac{16\pi\gamma^3 v_s^2}{3\Delta G_p^2}, \tag{3}$$

where γ is the interfacial tension between the A crystal and the fluid of composition X_A, ΔG_p is the free energy difference per particle between A in the fluid and A in the pure solid, and v_s is the volume per atom in the solid. Clearly, both γ and ΔG_p vary with fluid composition. ΔG_p is given by [37]

$$\Delta G_p = \frac{\Delta G_{nucl}}{N_A^{nucl}} = \mu_A^{fcc} - \mu_A^F. \tag{4}$$

μ_A^F is calculated by taking the intercept on the $X_A = 1{\cdot}0$ axis of the tangent to the fluid Gibbs free energy curve $G_F(X_A)$ at the composition X_A.

As the fluid becomes less rich in A spheres or, more generally, as its composition becomes less like the stoichiometry of the nucleating phase, the driving force for nucleation is lowered. This has the effect of lowering the nucleation rate for a fluid composition which differs markedly from that of the nucleating solid.

In order to examine whether this thermodynamic factor is sufficient to explain the apparent reluctance of A to crystallize from B-rich suspensions we have calculated the nucleation rate from the above expressions with the interfacial tension γ held constant. We have chosen the value of γ so that the packing fraction dependence of the rate of nucleation predicted for the one-component case parallels the observations made by Pusey *et al.* [18], i.e., nucleation commences just below the freezing density, and the rate of crystal formation is a maximum at $\phi \simeq 0{\cdot}53$. This gives $\gamma = 0{\cdot}2k_B T/\sigma^2$, which should be contrasted with the measured value of $0{\cdot}46k_B T/\sigma^2$ [40] and the theoretical value of $0{\cdot}61k_B T/\sigma^2$ [41] for a hard-sphere fluid against a planar hard-sphere wall. Using these larger values in the nucleation theory expression predicts crystallization only over a small range of densities, $\phi \simeq 0{\cdot}53$. The lower bound for observation of nucleation is then defined as 1/1000 of the maximum rate calculated for nucleation of f.c.c. A from a fluid of pure A at $\phi \simeq 0{\cdot}53$. The choice of criterion for nucleation does not affect significantly the variation of density at which nucleation is first adjudged to occur for differing fluid compositions. This is because the nucleation rate remains virtually zero until a critical density at which there is an 'explosion' of nuclei. Hence, a rather large range of choice for this lower limit to nucleation all 'pick out' this critical density quite well. Calculations based upon these considerations showed that the critical density for observation of nucleation does not depart significantly from the freezing line; i.e., they show that the simple

thermodynamic factor is not sufficient to block nucleation of A crystals from a B-rich suspension in the way apparently observed.

The other factor which might be involved in the blocking effect is the fluid composition dependence of the interfacial tension γ. Nothing is known about this dependence, although intuition would suggest that the strain at the interface should become greater as the difference in composition of the two phases increases. We have carried out illustrative calculations in which the surface free energy per unit area is allowed to vary linearly with composition from a value appropriate to pure A liquid–solid coexistence to pure B liquid–solid coexistence. This accounts only for the increasing number of the smaller B particles in a unit area of the interface, and is likely to underestimate the true variation. The results of this calculation are shown in figure 9. It can be seen that this line roughly divides the experimentally studied points at which nucleation of A was/was not observed. In view of the *ad hoc* treatment of the composition dependence of the interfacial term, all that can really be deduced from this figure is the great sensitivity of nucleation to surface, rather than bulk, thermodynamic effects.

5.2. *Icosahedral order in the fluid*

At a purely qualitative level, it seems reasonable to assert that a crystal will form readily from a fluid if the local order in the fluid resembles that in the crystal. In this case, the free energy barrier to crystallization would be expected to be low. Given the apparent readiness of AB_{13} crystals to nucleate, noted earlier, we have sought to characterize the local coordination structure in the fluid near to freezing. Jónsson and Andersen [42] have noted the presence of a significant degree of local icosahedral order in simulations of supercooled one- and two-component ($X_A = 0{\cdot}2$, $\sigma_B/\sigma_A = 0{\cdot}8$) Lennard-Jones systems. It seems possible that this local order could facilitate the formation of the locally icosahedral AB_{13} crystal. The icosahedral character of the AB_{13} crystal is very high: it is obvious that the B particle at the centre of an icosahedral unit is icosahedrally coordinated by 12 other B particles. What is less apparent is that the B particles on the outside of these clusters also have 12 neighbours, 10 B particles and two As, and that these are disposed icosahedrally. The central question to be addressed here is: does the presence of the A particles in fluids of composition close to AB_{13} induce a higher degree of icosahedral order around the B particles than would be found in a one-component fluid at the same packing fraction?

To answer this question we have examined a local bond-order parameter in simulations of pure A and AB_{13} fluids. As shown by Steinhardt *et al.* [43, 44] suitable, rotationally invariant, bond-order parameters may be constructed from combinations of spherical harmonics defined on the 'bond' connecting two atoms. To form a local order parameter for particle i, we construct

$$Q_{lm}^{i} = \frac{1}{N_b^i} \sum_{j=nn\ \text{bonds}} Y_{lm}(\boldsymbol{r}_{ij}), \tag{5}$$

where Y_{lm} is a spherical harmonic and $\boldsymbol{r}_{ij}$ is a unit vector directed along the line of centres of atoms i and j. The sum runs over those atoms which are closer than $1.2(\sigma_i + \sigma_j)$ and the number of contributions to the sum is N_b^i. Rotationally invariant combinations of the Q_{lm}^i are

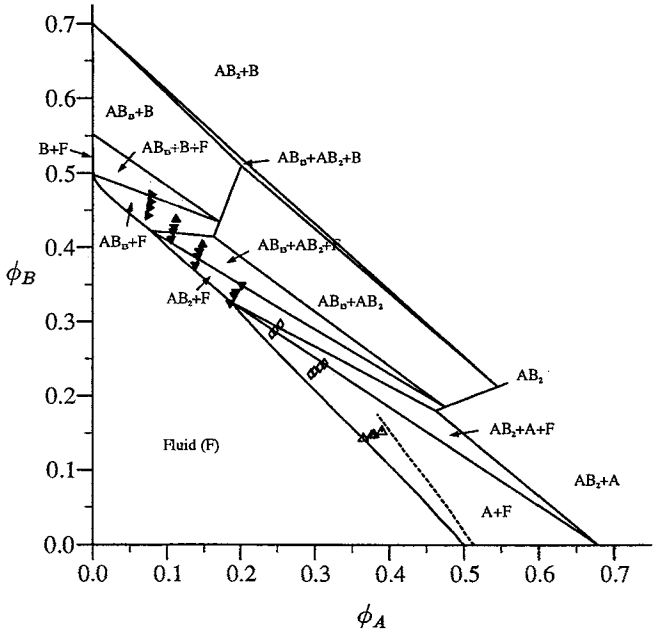

(*a*)

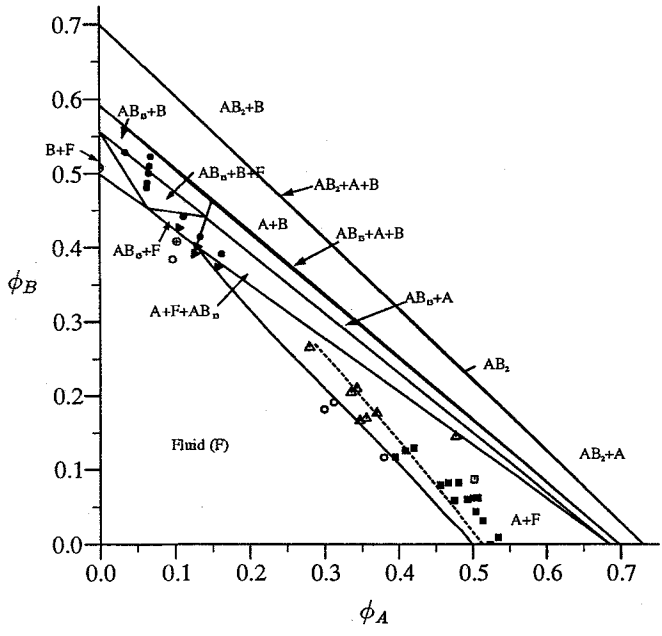

(*b*)

Figure 9. The dashed line shows the effect of the *ad hoc* composition dependent surface tension on the critical density for nucleation at both (*a*) $\alpha = 0{\cdot}58$ and (*b*) $\alpha = 0{\cdot}62$.

$$Q_l^i = \left(\frac{4\pi}{2l+1} \sum_{m=-l}^{l} |Q_{lm}^i|^2 \right)^{1/2}, \tag{6}$$

and

$$W_l^i = \sum_{\substack{m_1, m_2, m_3 \\ m_1+m_2+m_3=0}} \begin{pmatrix} l & l & l \\ m_1 & m_2 & m_3 \end{pmatrix} Q_{lm_1}^i Q_{lm_2}^i Q_{lm_3}^i. \tag{7}$$

Q_l^i is a second-order invariant and the bracketed term in the third-order invariant, W_l^i, is a Wigner-3j symbol. The ratio of these order parameters,

$$\hat{W}_l^i = W_l^i \Big/ \left(\sum_m |Q_{lm}^i|^2 \right)^{3/2}, \tag{8}$$

is found to be insensitive to the precise definition of neighbours used yet is a sensitive measure of different coordination symmetries.

By observing on a graphics terminal several clusters (of roughly 13 atoms) in dense fluid configurations the following criteria were found to indicate icosahedral order around a central particle i:

$$\left.\begin{aligned} Q_6^i &\geqslant 0{\cdot}40 \\ \hat{W}_6^i &\leqslant -0{\cdot}13 \\ 11 &\leqslant N_b^i \leqslant 13 \end{aligned}\right\} \text{icosahedral cluster.} \tag{9}$$

Similarly, the following criteria:

$$\left.\begin{aligned} Q_4^i &\geqslant 0{\cdot}10 \\ Q_6^i &\geqslant 0{\cdot}40 \\ \hat{W}_4^i &\leqslant -0{\cdot}12 \\ 11 &\leqslant N_b^i \leqslant 13 \end{aligned}\right\} \text{f.c.c. cluster,} \tag{10}$$

were applied in exploring configurations for f.c.c. clustering. In practice, we found that the particles identified by these criteria formed almost disjoint sets, and conformed well with the particles identified as icosahedrally or cubically coordinated on the graphics display.

Figure 10(*a*, *b*) shows the behaviour of the number N_I of icosahedrally and number N_C of cubically coordinated particles in two simulations as the fluids are gradually compressed to densities well above their equilibrium freezing densities. Compression simulations of this type are the hard sphere equivalent of temperature quenches in normal fluids. These fluids were gradually compressed in steps of $\Delta\phi = 0{\cdot}005$ separated by equilibration runs of 250 000 collisions up to a highest packing fraction, $\phi = 0{\cdot}60$. The compression itself was achieved by a sequence of small particle expansions accomplished by finding, after a 1000 collision sequence, what the maximum swelling of the particle radii would be in order to bring a pair of particles into contact and then swelling the particles by 90% of this value. Note that this means that the actual compression rate was not constant but became slower as the packing fraction became higher. Production runs of 500 000 collisions were performed for 16 densities in this range ($0{\cdot}45 \leqslant \phi \leqslant 0{\cdot}60$) from which averages of local order were taken.

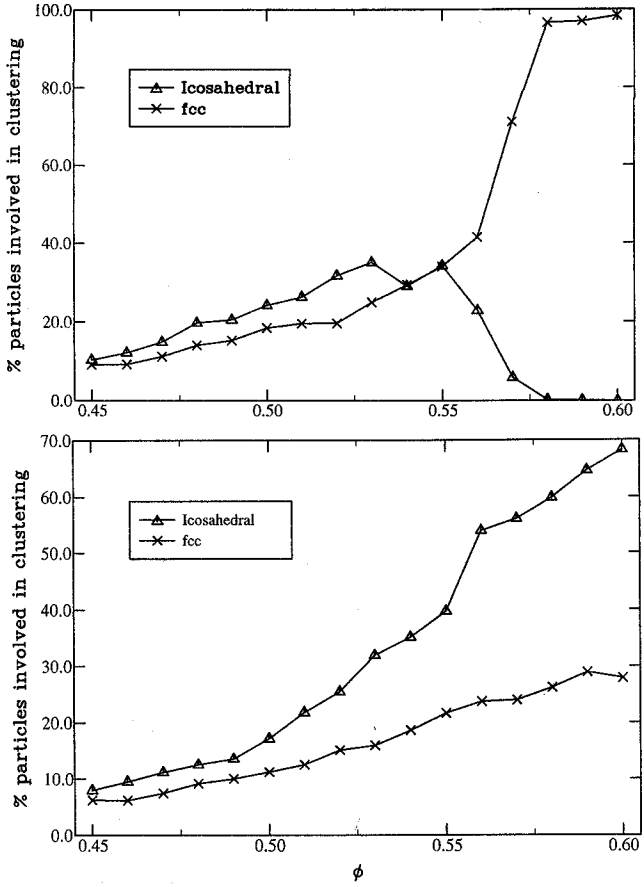

Figure 10. The percentage of particles involved in f.c.c. and icosahedral clustering in MD densification simulations for (*a*) a monodisperse hard-sphere system and (*b*) a binary hard-sphere mixture with $\alpha = 0{\cdot}58$ and $n_B/n_A = 13$.

For the one-component fluid compression, MD was performed on 864 particles in a cubic box. Figure 10(*a*) shows the average number of icosahedral and f.c.c. clusters found as the density was increased (this averaging was over 20 configurations output during the production run). The percentages of atoms involved in each cluster type are plotted in figure 10(*a*). As is clearly seen, icosahedral clustering does play a role in the dense hard-sphere fluid and reaches a peak for $\phi = 0{\cdot}55$ with an average of 34% involvement. However, in the one-component case, icosahedral order cannot be found in the crystalline phase, and f.c.c. clustering, which does lead to crystal nucleation, is a competing tendency. For $\phi \approx 0{\cdot}57$ the system crystallizes and the icosahedral order is swamped by the cubic order. Examination of the simulation cell at the end of this run showed that two close-packed crystallites had formed separated by grain boundaries. $\phi \approx 0{\cdot}57$ is the packing fraction identified by Woodcock as the limit of the metastable fluid branch under slow quenching conditions [7].

The second compression run was for a mixture with size ratio of $\alpha = 0{\cdot}58$, composition $X_A = 1/14$ corresponding to the AB_{13} stoichiometry, and total number

of particles $N = 896$. Figure 10(*b*) contrasts the behaviour of the AB_{13} fluid with the pure fluid case; again N_I and N_C rise smoothly together as ϕ is increased. However, in this case, even at packing fractions higher than the 'Woodcock' density, we do not see crystallization at the compression rates used. This accords with the experimental observation that crystallization is much slower in the binary mixtures than in one-component systems, i.e., that the crystalline state is more remote in some sense. (Close inspection of figure 10(*b*) shows a sharp jump in N_I at $\phi \simeq 0{\cdot}55$; we are currently examining whether this is linked to an incipient nucleation event in a series of runs at lower compression rates.) The noteworthy thing about these figures is that, at densities close to freezing, the degree of icosahedral order in the AB_{13} fluid is similar to that in the one-component case, i.e. there is no additional pre-ordering of the fluid at this composition above that which might be expected in a one-component system at the same density. The apparent relative ease of formation of the AB_{13} crystal in the binary mixtures, relative to the other possible crystal phases, must be due to the fact that a crystal with icosahedral local order is *possible* at this stoichiometry and size ratio which may be found by the intrinsic icosahedral fluctuations in the melt.

6. Conclusions

In this paper we have presented a detailed comparison between the phase behaviour found in a binary colloidal suspension of radius ratios 0·62 and 0·58, and an atomistic Monte Carlo simulation of a mixture of hard spheres. Our work is motivated by the recent observation of the spontaneous formation of two highly ordered superlattice structures, AB_2 and AB_{13}, in mixtures of colloidal spheres. Overall, we find a close level of agreement between simulation and experiment over wide regions of composition. In particular, simulation confirms the experimental result that the size ratio $\alpha = 0{\cdot}62$ is the upper limit for the stability of both superlattice phases. We also find excellent agreement between predictions for the densities and unit cell sizes and experiment. The quality of this agreement demonstrates that the effective potential between two colloidal particles is indistinguishable experimentally from the classical hard-sphere interaction. Consequently, factors such as the softness of the polymer coating or the polydispersity of the colloidal spheres are, at least in this case, unimportant.

In limited regions of composition we observe discrepancies between experiment and simulation. On the basis of the general level of agreement mentioned above, we attribute these differences to kinetic factors. A close comparison reveals several interesting non-equilibrium effects. First, the AB_{13} structure is very readily crystallized from a fluid phase, and second, by contrast, crystals of pure A and AB_2 are rather reluctant to crystallize from fluids which differ appreciably in composition from the pure solids. Utilizing results from Monte Carlo simulations we demonstrate that these trends may be explained in terms of the structural requirements for nucleation in these mixtures. The relatively rapid nucleation and growth of the icosahedral containing superlattice AB_{13} is most probably due to the large fraction (in excess of 40% at $\phi_A + \phi_B = 0{\cdot}55$) of particles in binary mixtures which are incorporated into 'icosahedral clusters' in the fluid phase. In contrast, the blocking of the nucleation of A and AB_2 is a consequence of the rapid variation of the interfacial energy, between crystal and fluid, with composition.

References

[1] BERNAL, J. D., 1960, *Nature*, **183**, 141; BERNAL, J. D., and MASON, J. 1960, *Nature*, **188**, 910; BERNAL, J. D., 1964, *Proc. R. Soc. Lond.* A, **280**, 299.
[2] SCOTT, G. D., 1960, *Nature*, **188**, 908.
[3] ALDER, B. J., and WAINWRIGHT, T. E., 1957, *J. chem. Phys.*, **27**, 1208.
[4] HOOVER, W. G., and REE, F. H., 1968, *J. chem. Phys.*, **49**, 3609.
[5] YOUNG, D. A., and ALDER, B. J., 1979, *J. chem. Phys.*, **70**, 473.
[6] FRENKEL, D., and LADD, A. J. C., 1984, *J. chem. Phys.*, **81**, 3188.
[7] WOODCOCK, L. V., 1981, *Ann. N.Y. Acad. Sci.*, **371**, 274.
[8] BAUS, M., and COLOT, J. L., 1985, *Molec. Phys.*, **55**, 653.
[9] FRENKEL, D., 1993, *Physics World*, February, 24.
[10] ACKERSON, B. J., 1993, *Nature*, **365**, 11.
[11] MURRAY, M. J., and SANDERS, J. V., 1980, *Phil. Mag.* A, **42**, 721.
[12] SANDERS, J. V., 1980, *Phil. Mag.* A, **42**, 705.
[13] HACHISU, S., and YOSHIMURA, S., 1987, *Physics of Complex and Supermolecular Fluids*, edited by S. A. Safran and N. A. Clark (New York: Wiley).
[14] TRIZAC, E., ELDRIDGE, M. D., and MADDEN, P. A., unpublished.
[15] KRANENDONK, W. G. T., and FRENKEL, D., 1991, *Molec. Phys.*, **72**, 679.
[16] BARRAT, J.-L., BAUS, M., and HANSEN, J.-P., 1986, *Phys. Rev. Lett.*, **56**, 1063; 1987, *J. Phys.* C, **20**, 1413.
[17] ELDRIDGE, M. D., 1993, D.Phil. Thesis, Oxford.
[18] PUSEY, P. N., *Liquids, Freezing and the Glass Transition*, edited by J.-P. Hansen, D. Levesque and J. Zinn-Justin (Amsterdam: Elsevier).
[19] DE KRUIF, C. G., JANSEN, J. W., and VRIJ, A., 1987, *Physics of Complex and Supermolecular Fluids*, edited by S. A. Safran and N. A. Clark, p. 315 (New York: Wiley).
[20] PUSEY, P. N., and VAN MEGEN, W., 1986, *Nature*, **320**, 340.
[21] BARTLETT, P., OTTEWILL, R. H., and PUSEY, P. N., 1990, *J. chem. Phys.*, **93**, 1299.
[22] BARTLETT, P., OTTEWILL, R. H., and PUSEY, P. N., 1992, *Phys. Rev. Lett.*, **68**, 3801.
[23] ELDRIDGE, M. D., MADDEN, P. A., and FRENKEL, D., 1993, *Nature*, **365**, 35.
[24] ELDRIDGE, M. D., MADDEN, P. A., and FRENKEL, D., 1993, *Molec. Phys.*, **79**, 105.
[25] ELDRIDGE, M. D., MADDEN, P. A., and FRENKEL, D., 1993, *Molec. Phys.*, **80**, 987.
[26] BARTLETT, P., 1990, *J. Phys.: Condens. Matter*, **2**, 4979.
[27] XU, H., and BAUS, M., 1992, *J. Phys.: Condens. Matter*, **4**, 663.
[28] BARTLETT, P., and VAN MEGEN, W., 1994, *Granular Matter, An Interdisciplinary Approach*, edited by A. Mehta (New York: Springer-Verlag), p. 195.
[29] ANTL, L., GOODWIN, J. W., HILL, R. D., OTTEWILL, R. H., OWENS, S. M., PAPWORTH, S., and WATERS, J. A., 1986, *Colloids Surfaces*, **17**, 67.
[30] PAULIN, S. E., and ACKERSON, B. J., 1990, *Phys. Rev. Lett.*, **64**, 2663.
[31] PUSEY, P. N., VAN MEGEN, W., BARTLETT, P., ACKERSON, B. J., RARITY, J. G., and UNDERWOOD, S. M., 1989, *Phys. Rev. Lett.*, **63**, 2753.
[32] BARTLETT, P., PUSEY, P. N., and OTTEWILL, R. H., 1991, *Langmuir*, **7**, 213.
[33] CAIRNS, R. J., OTTEWILL, R. H., OSMOND, D. W., and WAGSTAFF, I., 1976, *J. Colloid Interface Sci.*, **54**, 45.
[34] OTTEWILL, R. H., and LIVSEY, I., 1987, *Polymer*, **28**, 109.
[35] MANSOORI, G. A., CARNAHAN, N. F., STARLING, K. E., and LELAND, T. W., 1971, *J. chem. Phys.*, **54**, 1523.
[36] JACKSON, G., ROWLINSON, J. S., and VAN SWOL, F., 1987, *J. phys. Chem.*, **91**, 4907.
[37] PORTER, D. A., and EASTERLING, K. E., 1992, *Phase Transformations in Metals and Alloys* (London: Chapman & Hall).
[38] HAFNER, J., 1987, *From Hamiltonians to Phase Diagrams* (Berlin: Springer-Verlag).
[39] VAN MEGEN, W., and UNDERWOOD, S., 1993, *Nature*, **362**, 616.
[40] COURTEMANCHE, D. J., and VAN SWOL, F., 1992, *Phys. Rev. Lett.*, **69**, 2078.
[41] MARR, D. W., and GAST, A. P., 1993, *Phys. Rev.* E, **47**, 1212.
[42] JÓNSSON, H., and ANDERSEN, H. C., 1988, *Phys. Rev. Lett.*, **60**, 2295.
[43] STEINHARDT, P. J., NELSON, D. R., and RONCHETTI, M., 1983, *Phys. Rev.* B, **28**, 784.
[44] STEINHARDT, P. J., NELSON, D. R., and RONCHETTI, M., 1981, *Phys. Rev. Lett.*, **47**, 1297.